# Prediction of two stable freestanding $\beta_{12}$ borophanes: Structure, electronic properties, and superconductivity

Ying-Jie Chen,[1] Hong-Yan Lu ◉,[1,*] Feng-Lan Shao ◉,[1] and Ping Zhang[1,2,†]

[1]*School of Physics and Physical Engineering, Qufu Normal University, Qufu 273165, China*
[2]*Institute of Applied Physics and Computational Mathematics, Beijing 100088, China*

Borophene has several configurations and shows many unique properties, such as the Dirac point, the negative Poisson's ratio, inherent metallicity, but it is oxidized easily. Recently, ordered chemical modulation of $\beta_{12}$ borophene grown on the Ag(111) substrate by hydrogenation was experimentally reported, and three configurations of $\beta_{12}$ borophane were proposed by scanning tunneling microscopy and spectroscopy [Science **371**, 1143 (2021)]. In this paper, using first-principles calculations, we study seven configurations of hydrogen atoms adsorbed on freestanding $\beta_{12}$ borophene not only including the three adsorption structures in above literature, but also other four possible configurations with one or two hydrogen atoms adsorbed on it per unit cell. Among the seven configurations, we predict two stable $\beta_{12}$ borophanes. They possess the dynamic stability and different anisotropic metallicity from pristine $\beta_{12}$ borophene and show superconductivity. Based on the Eliashberg equation, the calculated electron-phonon coupling strength are about 0.82 and 0.52, and their superconducting transition temperature $T_c$ are 20.51 and 5.90 K, respectively. Thus, these borophanes provide new platforms for two-dimensional superconductivity and antioxidation of borophene.

## I. INTRODUCTION

The discovery of graphene and its unusual properties have made two-dimensional (2D) materials gain a widespread interest due to their large surface area and novel physical and chemical properties [1–10]. Boron (B), the neighbor of carbon (C), is in a special position of transition from metal to nonmetal in group IIIA of the periodic table. The electron configuration of its atomic ground state is $1s^2 2s^2 2p^1$, that is, three valence electrons in the outer layer to occupy four orbits, i.e., $2s$, $2p_x$, $2p_y$, $2p_z$, and it has electron-deficient characteristics, which makes B have strong chemical activity [11,12]. Therefore, B has a variety of allotropes including metal, semimetal, and semiconductor, showing rich electronic properties [13–17].

Borophene is a 2D material composed of single element B and monolayer atom. Due to the electron-deficient nature of B not only a two-center-two-electron bond can be formed in borophene, but also a multi-center-two-electron bond, such as the three-center-two-electron bond can be formed, leading to the structural diversity of borophene [18,19]. There are mainly two types of configurations predicted by theory: A triangular close-packed and a triangular and hexagonal mixed structure [20–22]. The first is nonplanar structure formed by some buckling B, and the second is the structure in which some B atoms are removed from the triangular dense lattice, leaving some hexagonal holes. The buckling or holes in both

structures can balance the electron-deficient character of the planar structure of B and improve the stability of borophene by enhancing electron delocalization [23,24].

In recent years, a variety of configurations of borophene have been prepared successfully [17,25–28]. They were theoretically predicted to show peculiar properties, such as the negative Poisson's ratio [29], inherent metallicity [30], optical transparency [31], high flexibility [32], and superconductivity [33–36]. The special physical and chemical properties of borophene may broaden its potential applications, such as hydrogen storage, battery, optically transparent electrode, etc. [37–40]. However, the thermodynamic, kinetic instability, and easy oxidation in air substantially limit its further development [25,26,41–47].

Functionalizing borophene [48,49], namely, adsorbing some atoms or groups, for instance, H, F, and OH on the surface of it, can effectively adjust its electronic properties, improve its stability and suppress ambient oxidation [15,50–54]. Particularly, it was recently reported that $\beta_{12}$ borophane polymorphs can be synthesized by hydrogenated $\beta_{12}$ borophene on an Ag(111) substrate under ultrahigh vacuum with the H atoms adsorbed on the same side of borophene [55]. Especially, three configurations of $\beta_{12}$ borophane on the Ag(111) substrate were proposed by the scanning tunneling microscopy and spectroscopy. Their results reveal that hydrogenation provides chemical passivation of borophane and reduces oxidation rates by more than two orders of magnitude after ambient exposure. Inspired by this, we adsorb different proportions of H atoms at different sites of freestanding $\beta_{12}$ borophene. It is anticipated to obtain the stable lattice structure and electronic properties of $\beta_{12}$ borophane through

---

*Corresponding author: hylu@qfnu.edu.cn
†Corresponding author: zhang_ping@iapcm.ac.cn

calculation, which can provide theoretical reference for improving the physical and chemical properties of $\beta_{12}$ borophene in experiments.

In this paper, by using the density functional theory (DFT), we found two stable configurations of hydrogenated free-standing $\beta_{12}$ borophene. Their lattice structures, bonding, electronic structures, phonon spectra, and superconductivity were studied in detail. Our results show that they are no longer pure planar structure but still maintain the anisotropy, dynamic stability, metallicity, and superconductivity. Most importantly, they should be antioxidants, compared with the pristine $\beta_{12}$ borophene according to the experimental results of Ref. [55].

## II. METHOD

In this paper, we applied the Vienna *ab initio* simulation package [56] within the framework of the DFT [57] to perform the structural relaxation and electronic properties. The electron-ion interaction was described by projector-augmented-wave pseudopotention [58]. The Perdew-Burke-Ernzerhof (PBE) functional theory under the generalized gradient approximation (GGA) [59,60] was chosen for the exchange-correlation function, and the plane-wave basis vector with the kinetic-energy cutoff of 400 eV was selected. The Brillouin zone was sampled with $7 \times 11 \times 1$ $\Gamma$-centered Monkhorst-Pack grids [61], so as to ensure that the total energy converges to 0.01 meV and the force converges to 0.03 eV/Å. A vacuum space of 20 Å was added to avoid interactions between adjacent layers. The phonon spectrum and electron-phonon interaction were calculated using the QUANTUM-ESPRESSO package [62]. All structures were reoptimized by the PBE functional and ultrasoft pseudopotential of GGA. Energy cutoffs of 80 and 800 Ry were set for the electronic-wave functions of a plane-wave basis and the charge density, respectively. The convergence criteria for the energy was set as $10^{-9}$ Ry. A $6 \times 10 \times 1$ $q$-point grid was set for calculating the phonon dispersion and phonon density of states, and an accurate electron-phonon interaction matrix was evaluated on a denser $24 \times 40 \times 1$ $k$-point grid. When estimating the superconducting critical temperature ($T_c$) using the McMillan-Allen-Dynes formula [63–65], we selected a typical value of the screened Coulomb repulsion constant $\mu^* = 0.1$, which was used for estimating $T_c$ of $\beta_{12}$ borophene [34,36].

## III. RESULTS AND DISCUSSIONS

### A. Structure and stability of hydrogenated $\beta_{12}$ borophene

The primitive cell of the freestanding $\beta_{12}$ borophene contains five B atoms (as shown in Fig. 1), which is a pure planar structure with a combination of closely arranged triangular and hexagonal holes. The filled and empty hexagon distribute along the zigzag direction. The optimized lattice constants are 5.08 and 2.92 Å, respectively, with the *Pmmm* (No. 47) space group. The results are consistent with the previous calculations [24,34–36,66]. Obviously, there are many possible sites for adsorbing H on its surface. We have explored multiple configurations of hydrogenated structures with one or two H atoms adsorbed on it per unit cell. The various
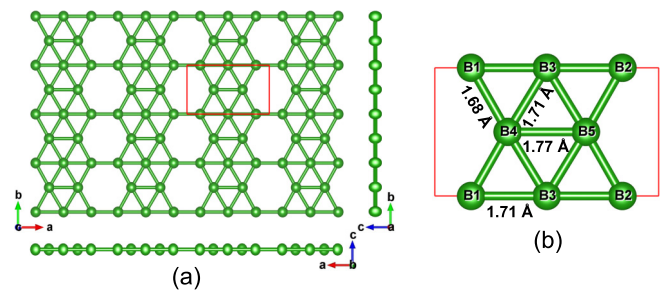


FIG. 1. (a) Top and side views of $\beta_{12}$ borophene. (b) Atomic number and B-B bond lengths labeled in the primitive cell. The green spheres represent the B atoms, and the red rectangle represents the primitive cell of $\beta_{12}$ borophene.

adsorbed structures after fully optimized are shown in Fig. 8 and their structure files are provided in the Supplemental Material [67]. The configurations with H atoms adsorbed on the same side can be synthesized by hydrogenating the $\beta_{12}$ borophene on the Ag(111) surface with atomic hydrogen sources in ultrahigh vacuum [55], whereas the borophanes with H atoms adsorbed on the opposite sides can be prepared by hydrogenating $\beta_{12}$ borophene via an *in situ* and three-step thermal-decomposition process, such as Ref. [68] when the freestanding $\beta_{12}$ borophene can be produced. It can be seen from Fig. 8 that the planar structure of $\beta_{12}$ borophene will fluctuate when it adsorbs H, which is an adaptive adjustment made by the borophene to improve its structural stability. In order to determine the stable configuration, we calculated the formation energy and phonon spectra of these structures.

Formation energy is a basic judgment index for evaluating the energy stability of materials. For $A_m B_n$-type material with $n$ B atoms adsorbed on the base material $A_m$ containing $m$ A atoms, its formation energy can be calculated by $E_{\text{form}} = E_{A_m B_n} - E_{A_m} - n E_B$. Here, $E_{A_m B_n}$ is the total energy of fully optimized $A_m B_n$, $E_{A_m}$ is the total energy of fully optimized base material $A_m$ and $E_B$ is the average monoatomic energy of substances in nature composed of B atoms, respectively. For the hydrogenated borophene, $E_{A_m B_n}$ and $E_{A_m}$ are the total energies of $\beta_{12}$ borophane and $\beta_{12}$ borophene, and $E_B$ is the average energy of the H atom in the $H_2$ molecule. The smaller the formation energy is, the more stable the structure is. The obtained formation energies for the structures in Fig. 8 are $E_{\text{top}} = 0.99$, $E_{\text{bridge 1}} = -0.10$, $E_{\text{bridge 2}} =$
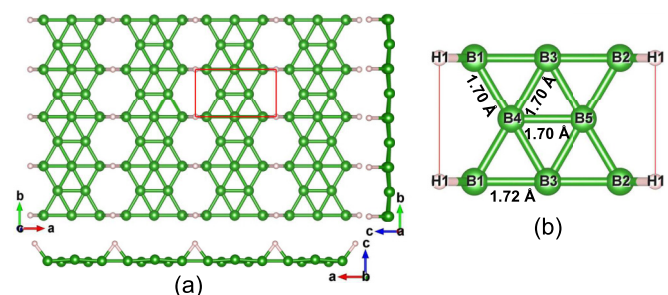


FIG. 2. (a) Top and side views of b1 borophane. (b) Atomic number and B-B bond lengths labeled in the primitive cell. The green and pink spheres represent B and H atoms, respectively. The red rectangle represents the primitive cell of it.
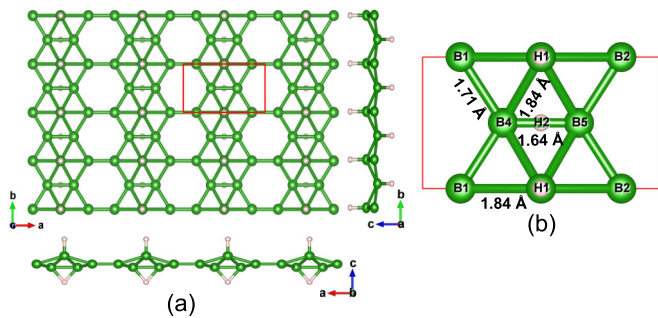
FIG. 3. (a) Top and side views of a hydrogenated t-b2 borophane. (b) Atomic number and B-B bond lengths labeled in the primitive cell. The green and pink spheres represent B and H atoms, respectively. The red rectangle represents the primitive cell of it.

$1.01$, $E_{\text{top+bridge 1}} = 0.48$, $E_{\text{top+bridge 2}} = 2.62$, $E_{\text{top-bridge 1}} = 0.74$, and $E_{\text{top-bridge 2}} = -0.30$ eV. It can be seen that the structures shown in Fig. 8(b) and 8(g) are relatively stable. Consequently, we calculated the phonon dispersions and total phonon density of states (PhDOS) of the hydrogenated configurations of borophene in Fig. 8 with the results shown in Fig. 9. According to the phonon spectra, the configurations in Figs. 8(b) and 8(g) where one H atom is adsorbed on the bridge site of B1-B2 (b) or two H atoms are adsorbed on the opposite sides of the boropene, i.e., on the bridge site of B4–B5 and the top site of B3 (g), are dynamically stable. Therefore, in the next section, we discuss the electronic properties of both borophanes, and focus on the analysis of the similarities and differences between the borophanes and the pristine $\beta_{12}$ borophene. For discussion purposes, we name them as b1 borophane and t-b2 borophane with the former similar to that reported by the experiment [55] but in the freestanding case.

The periodic structures of b1 borophane and t-b2 borophane are shown in Figs. 2 and 3. Compared with Fig. 1, it can be seen that the pure planar structure of borophene is changed. For b1 borophane, B3–B5 atoms have a slight displacement in the $c$-axis direction, whereas for t-b2 borophane, B4 and B5 atoms have a small displacement in addition to the larger
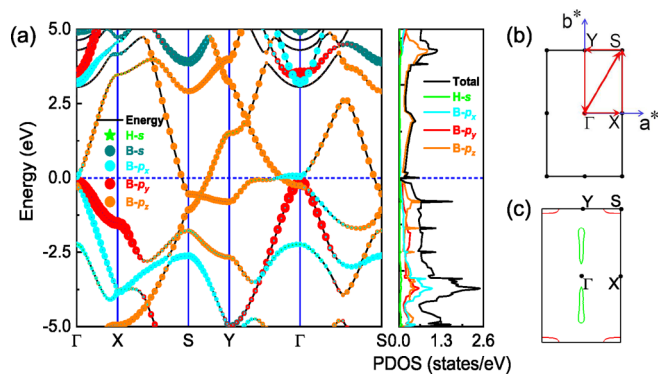


FIG. 4. (a) Orbital-projected electronic band structure (left), and total and partial electron density of states (right) of b1 borophane. The dotted line is the Fermi level (FL) set to zero. (b) The first Brillouin region of b1 borophane. (c) The Fermi surface (FS) of b1 borophane.
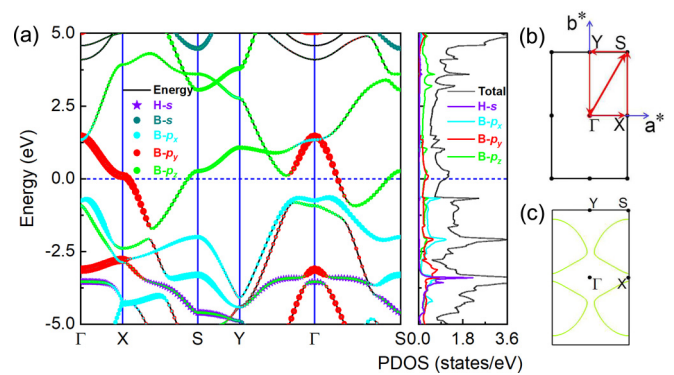


FIG. 5. (a) Orbital-projected electronic band structure (left), and total and partial electron density of states of t-b2 borophane (right). The dotted line is the FL set to zero. (b) The first Brillouin region of t-b2 borophane. (c) The FS of t-b2 borophane.

displacement of the B3 atom in the $c$-axis direction. The lattice constant of b1 borophane is almost unchanged ($a = 5.07$ and $b = 2.93$ Å), and the length of $a$ of t-b2 borophane increases slightly ($a = 5.12$ Å) and its length of $b$ decreases slightly ($b = 2.85$ Å) compared with those of the pristine borophene ($a = 5.08$, $b = 2.92$ Å). It can also be seen from Figs. 2(b), and 3(b) that B bonds with H, and the B-B bond length has changed accordingly, and then the borophanes are anisotropic in the $a$-, $b$-, and $c$-axis directions with space-group $Pmm2$ (No. 25). The bond lengths of B1-H1 in b1 borophane is 1.36 Å, whereas those of B3-H1 and B4(B5)-H2 in t-b2 borophane are 1.20 and 1.36 Å, respectively, which are close to those in two-centers-two-electrons bond (1.19 Å) and three-centers-two-electrons bond (1.31 Å) in Refs. [55,69], indicating that H and B in the borophanes form a covalent bond. As can be seen from Figs. 2(b), 3(b) and 1(b), the adsorption of H also changes the corresponding B-B bond length in the pristine borophene: The B4-B5 bond lengths of b1 and t-b2 borophane become significantly shorter, the B3-B4 bond lengths of b1 borophane become slightly longer, and other bond lengths become longer. This adjustment will lead to the redistribution of electrons. The difference of electron distribution will be revealed in a later analysis.

## B. Electronic properties of $\beta_{12}$ borophane

To probe the influences of the structural change on the electron distribution of borophene, we performed the Bader charge analysis of borophene and borophanes as shown in Figs. 10(a)–10(c). The figures show the estimated net charge of per atom. Positive (negative) numbers represent the net charge lost (gained) by the atom. Comparing Figs. 10(a)–10(c), for the pristine borophene, the positively and negatively charged B atoms are arranged alternately along the $b$-axis direction of the primitive cell. After adsorbing H atoms, the net charge transfers from B to H atoms, forming a stable covalent bond between B and H atoms. Particularly, in t-b2 borophane, the $H_{\text{top}}$ atom is more negatively charged than the $H_{\text{bridge}}$ atom. Otherwise, Fig. 10 also shows that the electrons on B atoms are redistributed after adsorbed H atoms, which should be the reason why the borophane has antioxidation. The borophane's
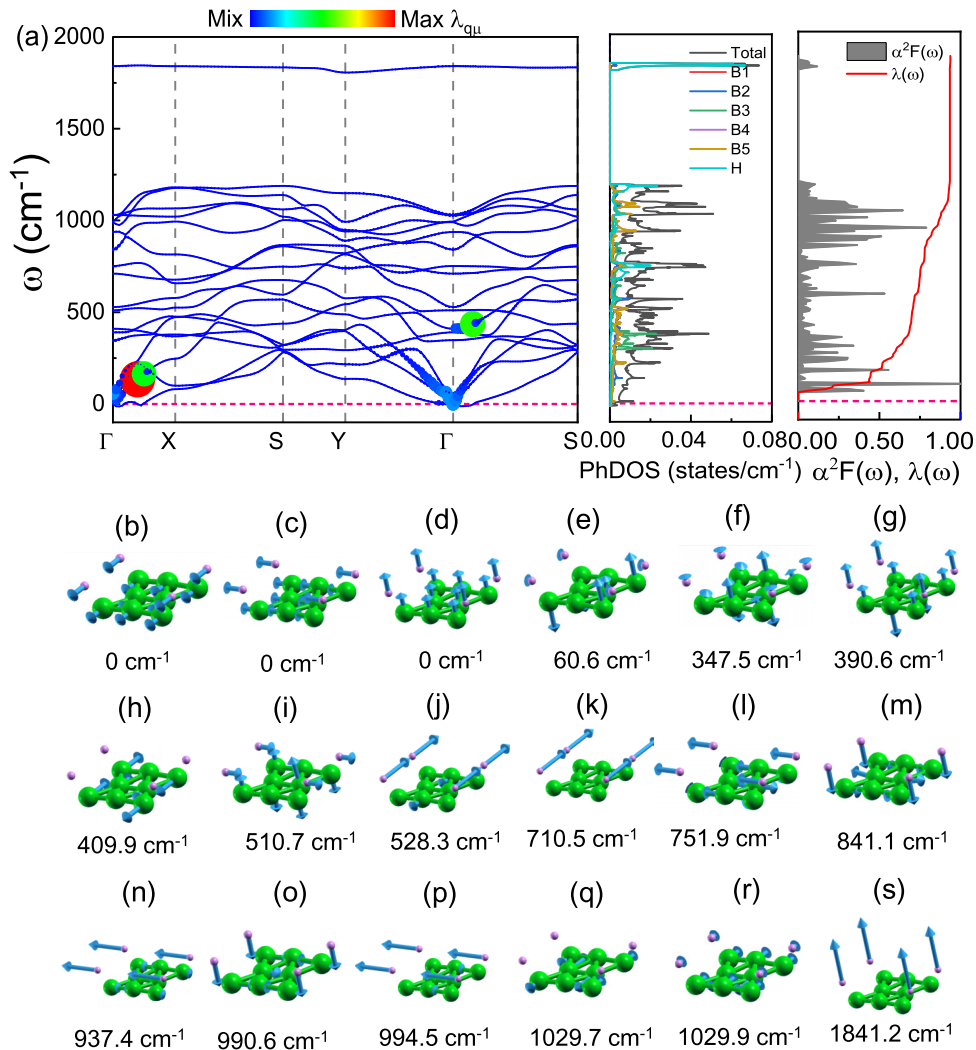
FIG. 6. (a) Phonon dispersion weighted by the magnitude of electron-phonon coupling (EPC) $\lambda_{qv}$, total and projected PhDOS, the Eliashberg spectral function $\alpha^2 F(\omega)$, and EPC $\lambda(\omega)$ of b1 borophane. (b)–(s) The vibration modes at the $\Gamma$ point.

antioxidation has been experimentally verified in Ref. [55]. In addition, there are many researches which have showed that chemical passivation can suppress ambient oxidation for electronic materials. For instance, monohydride termination of the dangling bonds on silicon surfaces minimizes native oxide formation [70,71], and covalent modification of 2D black phosphorus improves morphological stability and preserves electronic properties in ambient conditions [72]. In order to clearly understand the bonding nature in $\beta_{12}$ borophene and $\beta_{12}$ borophanes, we calculated the electron localization function (ELF) of them as illustrated in Figs. 11–13.

The value of ELF is between 0 and 1, which reflects the degree of charge localization in the real space and helps to understand the characterictics of the chemical bonds. 0 corresponds to the free electronic state, whereas 1 indicates a perfect localization, and 0.5 indicates homogeneous electron gas. As illustrated in Figs. 11–13, high ELF values are distributed between B atoms and around H atoms, indicating the presence of B-B and B-H and B-H-B covalent bonds. Therefore, Figs. 10(a)–10(c) show that the charge tends to

accumulate around the adsorbed H atoms in hydrogenated borophene. Maybe, this peculiar bonding feature can make the borophanes show antioxidant property as other kinds of borophanes in Ref. [55].

Next, we analyze the influence of hydrogenation on the electronic band structure of $\beta_{12}$ borophene. For this purpose, we calculated the orbital-projected electronic band structure as well as total and partial electron density of states (PDOS) of b1 and t-b2 borophane and borophene, which are shown in Figs. 4, 5, and 14. The results of borophene shown in Fig. 14 reveals that it is metallic, which is consistent with previous results and is also mutually confirmed with the significant DOS near its FL measured by scanning tunneling spectroscopy [33–36]. Normally, the out-of-plane $\pi$ bonds originated from $p_z$ orbitals are weaker than the in-plane bonds formed from $sp^2$ hybridization, hence, a structure that optimally filling the in-plane states should be the most desirable [20]. Figure 14(a) shows that almost all states of the in-plane orbitals are filled, and the remaining electrons fill in the $\pi$ state of the out-of-plane $p_z$ orbitals around the FL. The FL
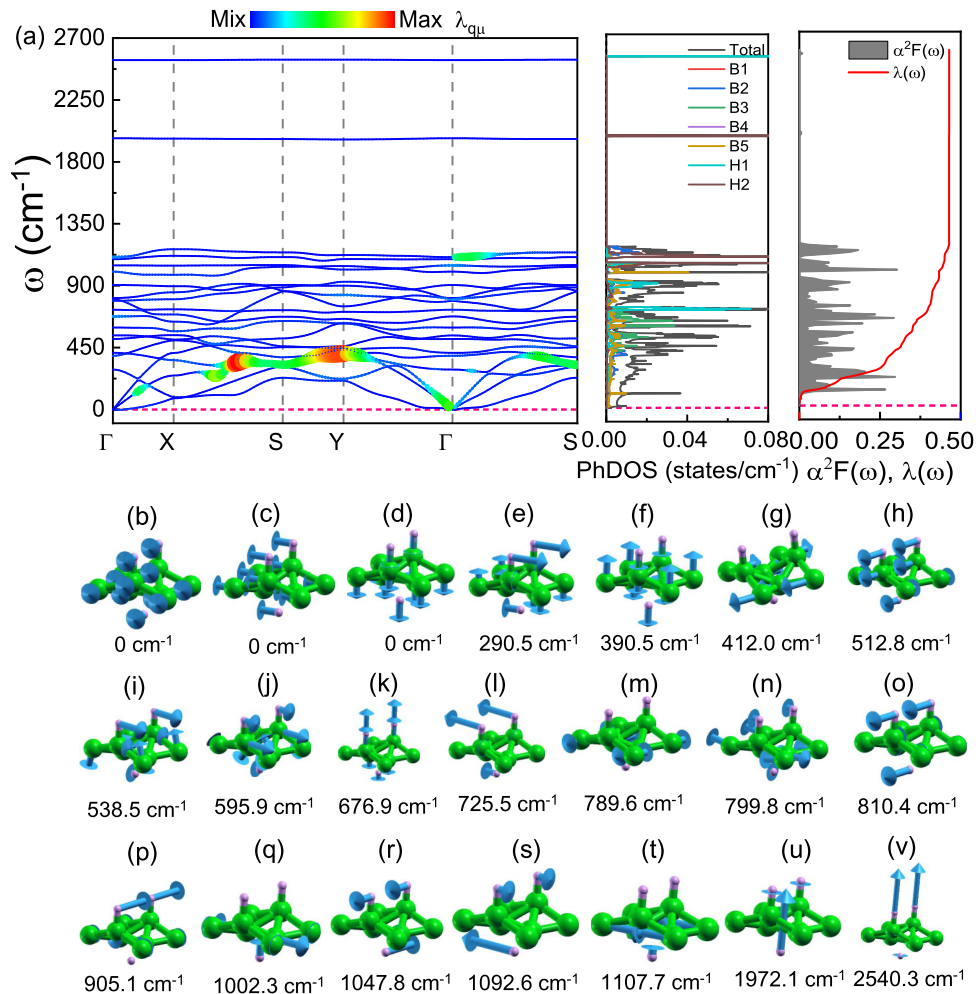
FIG. 7. (a) Phonon dispersion weighted by the magnitude of EPC $\lambda_{qv}$, total and projected PhDOS, the Eliashberg spectral function $\alpha^2 F(\omega)$, and EPC $\lambda(\omega)$ of t-b2 borophane. (b)–(v) The vibration modes at the $\Gamma$ point.

passes through three bands filled with $p_x$, $p_y$ and $p_z$ electrons. Accordingly, the FS of borophene in Fig. 14(c) shows two main features: (i) two small hole pockets at the $\Gamma$ point (two circulars) are composed of bonded boron $p_x$ and $p_y$ orbitals, (ii) a large ellipselike electron pocket is centered on Y composed of $p_z$ orbitals. When borophene adsorbs H atoms, its electronic structure changes significantly (see Figs. 4 and 5). Figures 4(a) and 5(a) show that b1 and t-b2 borophane are still metallic, but the number of electronic bands passing through the FL have changed from three to two, and the two bands are partially filled with $p_x$- and $p_z$- (for b1 borophane) or $p_y$- and $p_z$-orbital electrons (for t-b2 borophane). At the same time, the electronic states related to the $p_y$ or $p_x$ orbitals have been fully occupied, which is also verified by the PDOS on the right side of Figs. 4(a) and 5(a). Meanwhile, the FS shape has also changed greatly. The small hole pockets around $\Gamma$ disappears. Compared with borophene, b1 and t-b2 borophanes show different anisotropies. Furthermore, as pointed out in Refs. [20,50], the in-plane bond formed by overlapping $sp^2$ hybridization is stronger than the out-of-plane $\pi$ bond formed by $p_z$-orbital electrons. Here, the electrons near the FL occupy more $p_y$ orbital and less out-of-plane $p_z$ orbital

in the borophanes. Besides, the adsorption of H atoms makes the triple-center bonds and double-center bonds appear in the borophanes, so it can be speculated that this is why b1 and t-b2 borophane are more stable and antioxidant than the pristine borophene.

### C. Superconductivity of $\beta_{12}$ borophane

References [34–36] have proved that $\beta_{12}$ borophene shows superconductivity, which is also verified by our calculation. In order to analyze the influence of H adsorption on its superconductivity, we calculated the superconducting transition temperature of the borophene and borophanes. The results are shown in Figs. 6, 7, and 15. Figure 15(a) shows the phonon dispersion, the projected PhDOS, the Eliashberg spectral function $\alpha^2 F(\omega)$, and electron-phonon coupling $\lambda(\omega)$ of the pristine borophene. The phonon dispersion in Fig. 15(a) is consistent with that in Ref. [36] except for the appearance of small imaginary phonon frequency of the transverse branch near $\Gamma$, which was also found in two other Refs. [33,35]. The occurrence of the imaginary frequency was usually attributed to the numerical difficulties in accurate calculation of rapid
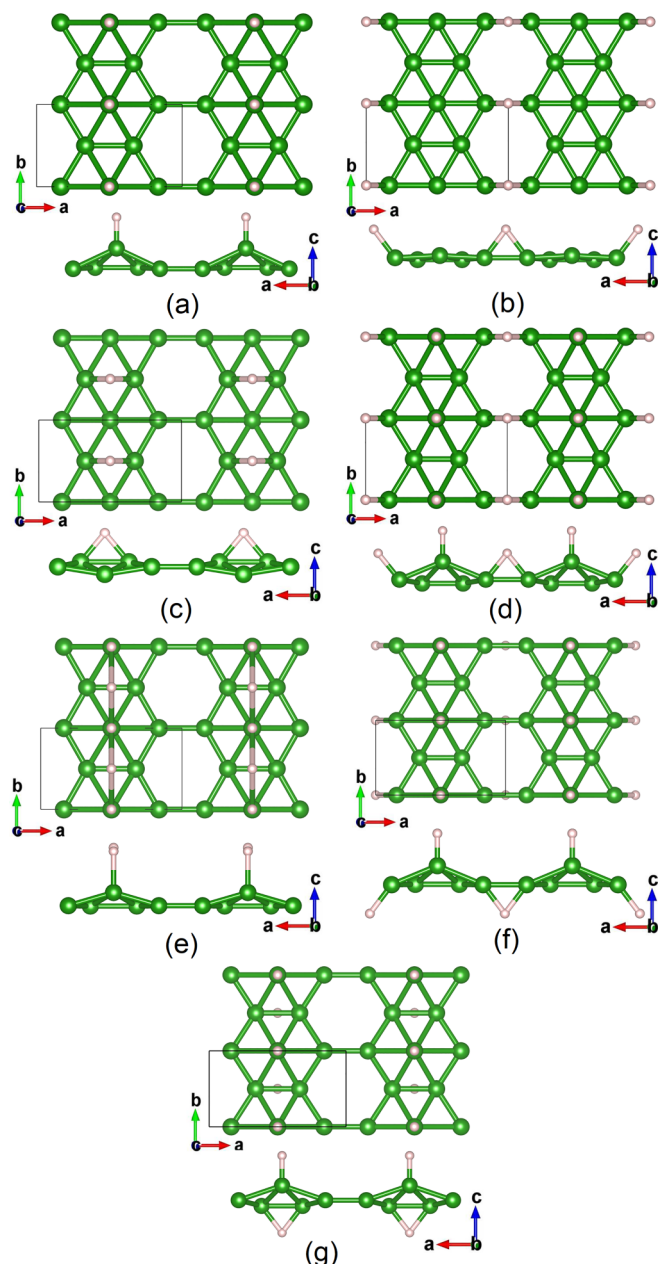
(a)

(b)

(c)

(d)

(e)

(f)

(g)

FIG. 8. Top and side views for various configurations of H adsorbed by $\beta_{12}$ borophene on the same or different sides of bridge and top positions: (a) top site; (b) bridge 1 site; (c) bridge 2 site; (d) top+bridge 1 site; (e) top + bridge 2 site; (f) top-bridge 1 site; (g) top-bridge 2 site. Where "+" means on the same side, "−" means on different sides. The green and pink spheres represent B and H atoms, respectively. The black rectangle is the primitive cell of each structure.

decaying interatomic forces and is not a sign of structural transition [73].

As shown in the rightmost figure of Fig. 15(a), the vibration mode below 400 cm$^{-1}$ contributes to the main EPC, and the EPC strength accounts for about 80% of the total EPC strength (total $\lambda = 0.82$). The logarithmic average of the phonon frequencies $\omega_{\log}$ is 298.64 K and the superconducting transition temperature $T_c$ is 14.59 K using $\mu^* = 0.1$. Specifically, the
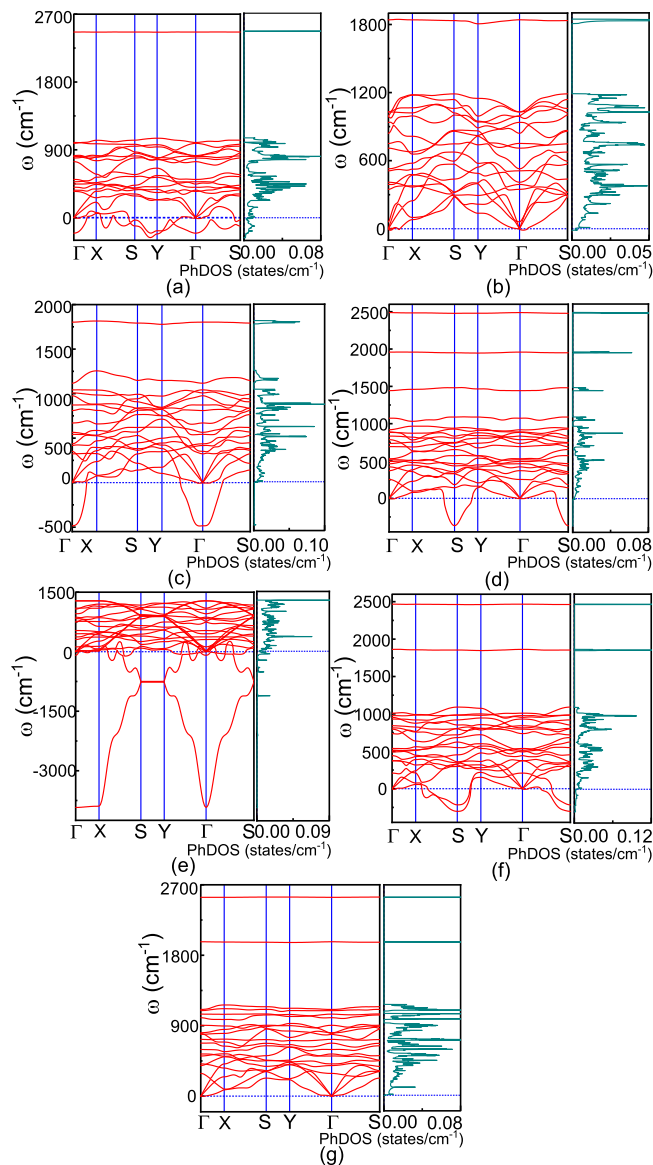


FIG. 9. Phonon dispersions and total PhDOS of the hydrogenated configurations of $\beta_{12}$ borophene in Fig. 8.

out-of-plane vibrations of B atoms below 400 cm$^{-1}$ are responsible for the Eliashberg spectral function $\alpha^2 F(\omega)$ and the PhDOS [Figs. 15(b)–15(p)].
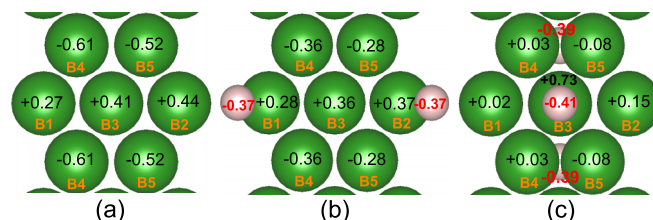


FIG. 10. Estimated net charge on B (green) and H (pink) atoms based on the Bader charge analysis for (a) $\beta_{12}$ borophene, (b) b1 borophane, and (c) t-b2 borophane. The black (red) numbers represent the net charge on B (H) atoms.
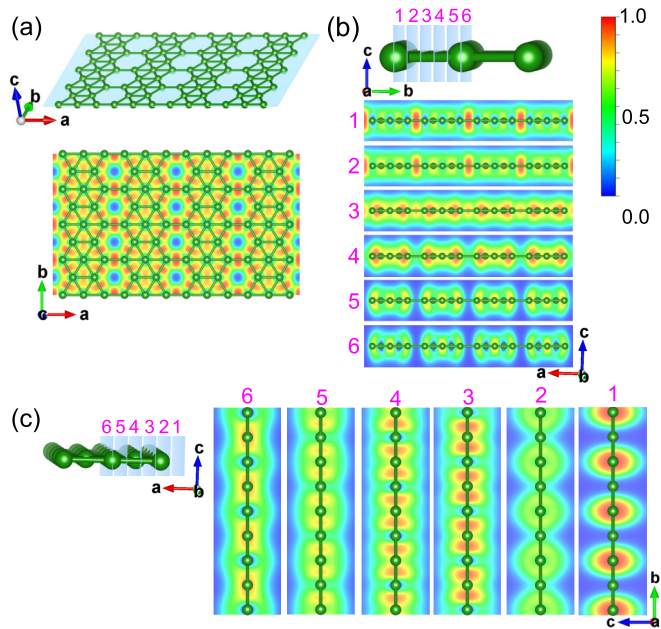
FIG. 11. Electron localization functions on crystal planes in different directions in $\beta_{12}$ borophene. The Arabic numbers in the violet box are the serial numbers of the corresponding sections.

After hydrogenation, for b1 borophane as shown in Fig. 6, the frequency range of the phonon spectra is greatly expanded (from 0 to 1117.8 cm$^{-1}$ of the pristine borophene to 0 to 1834.3 cm$^{-1}$) and the high-frequency branches come entirely from the contribution of H atoms, but the electron-phonon coupling is still mainly contributed by the lower-frequency vibration modes. The EPC strength in the range of 0–400 cm$^{-1}$ accounting for 74% and its out-of-plane vibrations below 400 cm$^{-1}$ are responsible for the Eliashberg spectral function $\alpha^2 F(\omega)$ and the PhDOS [Figs. 6(b)–6(s)]. The calculated $\lambda$ and $\omega_{\log}$ are 0.82 and 414.61 K, respectively, which are the



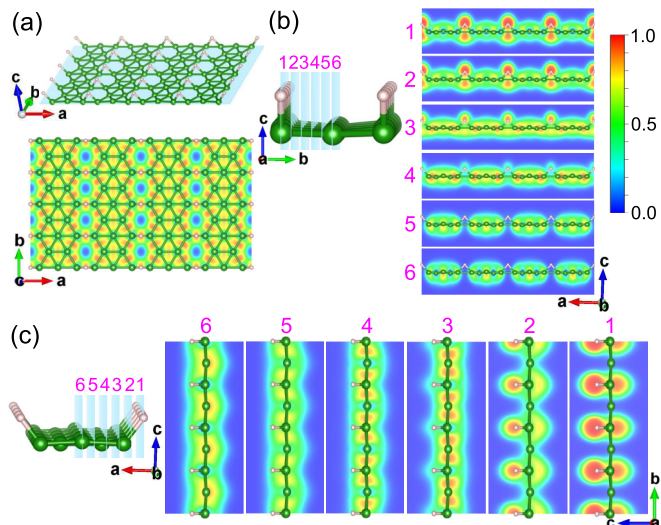FIG. 12. Electron localization functions on crystal planes in different directions in b1 borophane. The Arabic numbers in the violet box are the serial numbers of the corresponding sections.
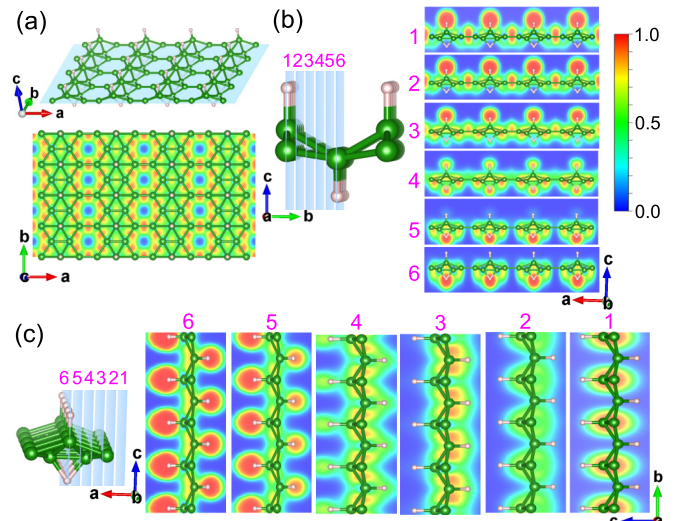


FIG. 13. Electron localization functions on crystal planes in different directions in t-b2-borophane. The Arabic numbers in the violet box are the serial numbers of the corresponding sections.

same and higher than those of the pristine case. According to the McMillan-Allen-Dynes formula, the calculated $T_c$ is 20.51 K, which is higher than that of the pristine borophene.

For t-b2 borophane, its phonon spectrum is also dramatically increased (from 0 to 1117.8 cm$^{-1}$ of the pristine borophene to 0 to 2543.1 cm$^{-1}$) with the high-frequency branches contributed by the vibrations of H atoms. However, the EPC still mainly originates from the lower-frequency vibration modes, and the EPC strength in the range of 0–400 cm$^{-1}$ accounts for 64% of the total $\lambda$. Meanwhile, from Figs. 7(b)–7(v), one can see that the low-frequency in-plane and out-of-plane vibration modes compete with each other. And then the calculated $\lambda$ and $\omega_{\log}$ are 0.52 and 429.95 K, respectively, which are lower and higher than those of the pristine case. According to the McMillan-Allen-Dynes formula, the calculated $T_c$ is 5.90 K, which is smaller than that of the pristine borophene.

Therefore, hydrogenation can not only improve the electronic structure of borophene, but also change its supercon-
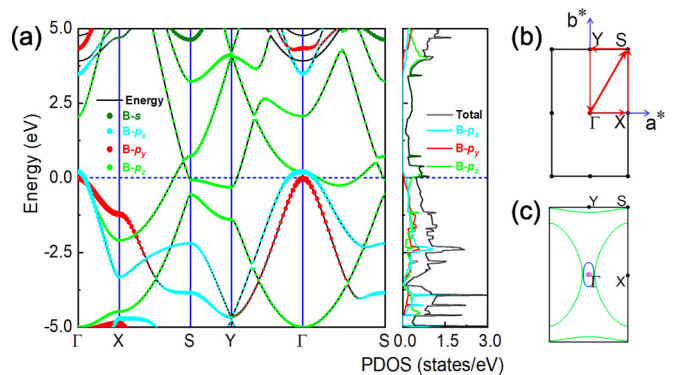


FIG. 14. (a) Orbital-projected electronic band structure and total and partial electron density of states of $\beta_{12}$ borophene (right). The dotted line is the FL which is set to zero. (b) The first Brillouin region of $\beta_{12}$ borophene. (c) The FS of $\beta_{12}$ borophene.
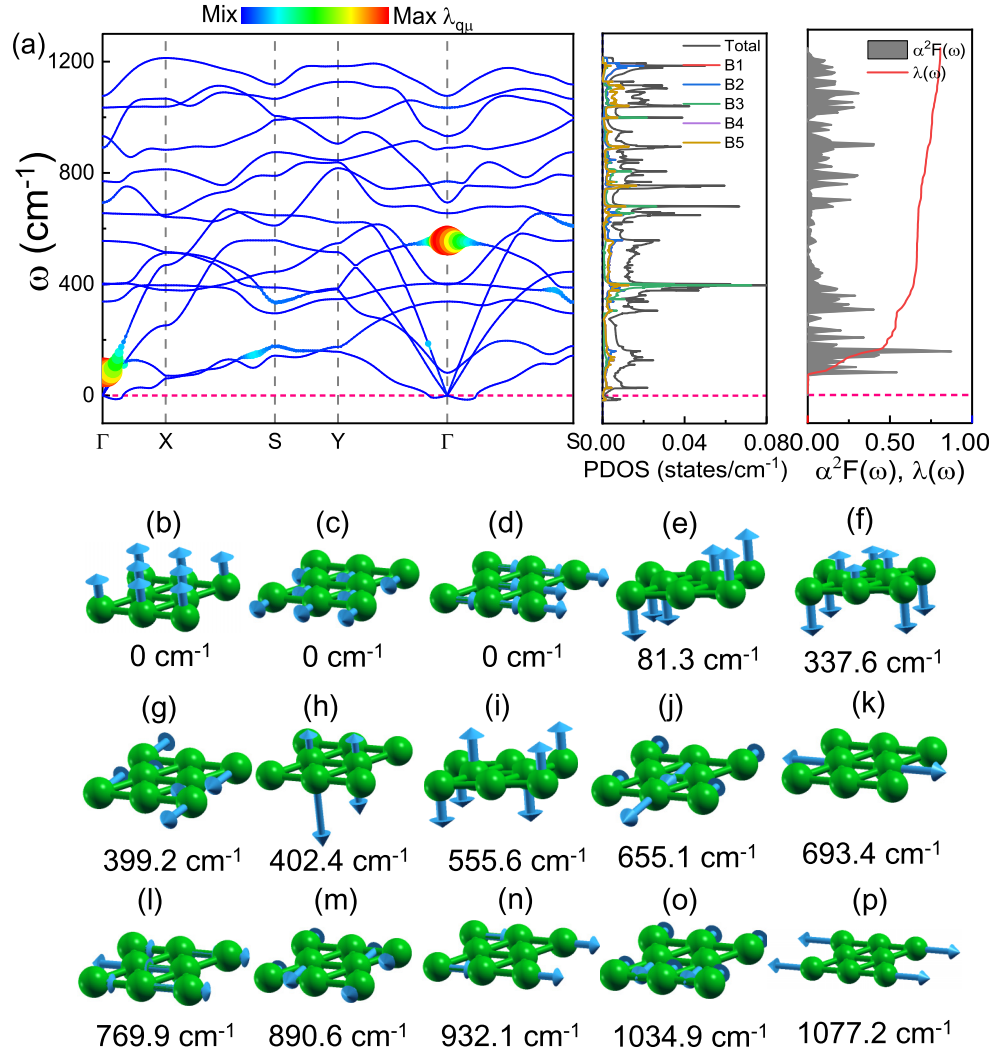
FIG. 15. (a) Phonon dispersion weighted by the magnitude of EPC $\lambda_{qv}$, total and projected PhDOS, Eliashberg spectral function $\alpha^2 F(\omega)$, and EPC $\lambda(\omega)$ of $\beta_{12}$ borophene. (b)–(p) The vibration modes at the $\Gamma$ point.

ductivity. The different adsorption sites make the vibration modes of borophanes significantly different. When hydrogen atoms are only adsorbed on the bridge site (for b1 borophane), the low-frequency out-of-plane vibration modes of borophane make a greater contribution to the EPC of b1 borophane. However, when hydrogen atoms are adsorbed on both sides of the bridge and the top (for t-b2 borophane), although hydrogen adsorption makes the borophene more stable, the lower-frequency in-plane and out-of-plane vibration modes compete with each other, which, in turn, makes the superconductivity of borophane weaker.

## IV. CONCLUSION

To summarize, we have studied the properties of the two stable configurations of hydrogenated freestanding $\beta_{12}$ borophene in detail. We analyzed their dynamic stability, electronic structure, and superconductivity then found the following conclusions: (1) The adsorption of H atoms has little effect on the lattice constant of borophene, but it wrinkles the planar structure of pristine borophene, so the bond length of some B-B bonds increases or decreases; (2) in b1 borophane

and t-b2 borophane, the H obtains electrons from its nearest B neighbors, and a large number of electrons are localized around the H, which changes the bonding mode of pristine borophene and forms strong B-H and B-H-B bonds. The two-center-two-electron and three-center-two-electron covalent bonds play an important role in stabilizing the structure and antioxidation of borophanes; (3) the two borophanes are still in metallic state, but the band structure and the FS are significantly changed compared with those of $\beta_{12}$ borophene; (4) the calculated electron-phonon coupling strength are about 0.82 and 0.52, and the superconducting transition temperature $T_c$ are 20.51 and 5.90 K, respectively. Thus, the predicted borophane provides a new platform for realizing 2D superconductivity and antioxidation of borophene.

Introduction and Cultivation for Young Innovative Talents in Colleges and Universities of Shandong Province.

## APPENDIX A: MULTIPLE STRUCTURES OF HYDROGENATED $\beta_{12}$ BOROPHENE

In Ref. [55], the properties of hydrogenated $\beta_{12}$ borophene on the Ag(111) substrate was experimentally investigated, which is not enough to characterize the features of the freestanding sample after hydrogenation. Therefore, we study the properties of several hydrogenated configurations of $\beta_{12}$ borophene, which are shown in Fig. 8.

## APPENDIX B: STABILITY OF HYDROGENATED $\beta_{12}$ BOROPHENE

The phonon dispersions and the total PhDOS of the hydrogenated configurations of $\beta_{12}$ borophene in Fig. 8 are calculated and shown in Fig. 9. The results reveal that the configurations bridge 1 and top-bridge 2 in Figs. 8(b) and 8(g) where one H or two H atoms are adsorbed on the side of the bridge B1-B2 or opposite sides of the bridge B4-B5 and top B3, respectively, are the dynamically stable in all the configurations that we have proposed.

## APPENDIX C: CHARGE DISTRIBUTION AND CHARGE LOCALIZATION

The Bader charge analysis of $\beta_{12}$ borophene, $\beta_{12}$ b1 and t-b2 borophane are shown in Fig. 10. Meanwhile, the ELF of them are illustrated in Figs. 11–13.

## APPENDIX D: ELECTRONIC BAND STRUCTURE AND TOTAL AND PARTIAL ELECTRON DENSITY OF STATES OF $\beta_{12}$ BOROPHENE

Figure 14, showing that borophene is metallic, is consistent with the previous results [33–36]. Meanwhile, Fig. 14(a) shows that almost all states of in-plane orbitals are filled, and the remaining electrons fill in the $\pi$ state of the out-of-plane $p_z$ orbitals around the FL. The FL passes through three bands filled with $p_x$, $p_y$, and $p_z$ electrons.

## APPENDIX E: PHONON DISPERSION OF $\beta_{12}$ BOROPHENE

Figure 15 shows the projected PhDOS, the Eliashberg spectral function $\alpha^2 F(\omega)$, EPC $\lambda(\omega)$, and the vibration mode with greater contribution to the EPC of borophene. The phonon dispersion of Fig. 15(a) is consistent with that in Refs. [34,36].

[1] K. S. Novoselov, A. K. Geim, S. V. Morozov, D. Jiang, Y. Zhang, S. V. Dubonos, I. V. Grigorieva, and A. A. Firsov, Science **306**, 666 (2004).

[2] A. H. Castro Neto, F. Guinea, N. M. R. Peres, K. S. Novoselov, and A. K. Geim, Rev. Mod. Phys. **81**, 109 (2009).

[3] F. Ersan, D. Kecik, V. O. Ozcelik, Y. Kadioglu, O. U. Akturk, E. Durgun, E. Akturk, and S. Ciraci, Appl. Phys. Rev. **6**, 021308 (2019).

[4] C. Chang, W. Chen, Y. Chen, Y. H. Chen, Y. Chen, F. Ding, C. H. Fan, H. J. Fan, Z. X. Fan, and C. Gong *et al.*, Acta Phys. Chim. Sin. **37**, 2108017 (2021).

[5] K. Cao, S. Z. Feng, Y. Han, L. B. Gao, T. H. Ly, Z. P. Xu, and Y. Lu, Nat. Commun. **11**, 284 (2020).

[6] T. A. Chen, C. P. Chuu, C. C. Tseng, C. K. Wen, H. S. P. Wong, S. Y. Pan, R. T. Li, T. A. Chao, W. C. Chueh, Y. F. Zhang, Q. Fu, B. I. Yakobson, W. H. Chang, and L. J. Li, Nature (London) **579**, 219 (2020).

[7] A. VahidMohammadi, J. Rosen, and Y. Gogotsi, Science **372**, 1165 (2021).

[8] A. Sebastian, R. Pendurthi, T. H. Choudhury, J. M. Redwing, and S. Das, Nat. Commun. **12**, 693 (2021).

[9] L. Wang, Y. P. Shi, M. F. Liu, A. Zhang, Y. L. Hong, R. H. Li, Q. Gao, and M. X. Chen, W. C. Ren, H. M. Cheng, Y. Y. Li, and X. Q. Chen, Nat. Commun. **12**, 2361 (2021).

[10] A. Ahmed, S. Sharma, B. Adak, M. M. Hossain, A. M. Lachance, S. Mukhopadhyay, and L. Y. Sun, InfoMat **4**, 28 (2022).

[11] A. R. Oganov, J. Chen, C. Gatti, Y. Ma, Y. Ma, C. W. Glass, Z. Liu, T. Yu, O. O. Kurakevych, and V. L. Solozhenko, Nature (London) **457**, 863 (2009).

[12] F. Ma, Y. Jiao, G. Gao, Y. Gu, A. Bilic, Z. Chen, and A. Du, Nano Lett. **16**, 3022 (2016).

[13] Z. A. Piazza, H. S. Hu, W. L. Li, Y. F. Zhao, J. Li, and L. S. Wang, Nat. Commun. **5**, 3113 (2014).

[14] X. F. Zhou, X. Dong, A. R. Oganov, Q. Zhu, Y. Tian, and H. T. Wang, Phys. Rev. Lett. **112**, 085502 (2014).

[15] Y. Jiao, F. X. Ma, J. Bell, A. Bilic, and A. Du, Angew. Chem., Int. Ed. **128**, 10448 (2016).

[16] S. Jalife, L. Liu, S. Pan, J. L. Cabellos, E. Osorio, C. Lu, T. Heine, K. J. Donald, and G. Merino, Nanoscale **8**, 17639 (2016).

[17] B. J. Feng, J. Zhang, R. Y. Liu, T. Iimori, C. Lian, H. Li, L. Chen, K. H. Wu, S. Meng, F. Komori, and I. Matsuda, Phys. Rev. B **94**, 041408(R) (2016).

[18] J. K. Olson and A. I. Boldyrev, Chem. Phys. Lett. **523**, 83 (2012).

[19] T. Ogitsu, E. Schwegler, and G. Galli, Chem. Rev. **113**, 3425 (2013).

[20] H. Tang and S. Ismail-Beigi, Phys. Rev. Lett. **99**, 115501 (2007).

[21] X. Yang, Y. Ding, and J. Ni, Phys. Rev. B **77**, 041402(R) (2008).

[22] W. L. Li, X. Chen, T. Jian, T. T. Chen, J. Li, and L. S. Wang, Nat. Rev. Chem. **1**, 0071 (2017).

[23] Y. Wang, Y. Park, L. Qiu, I. Mitchell, and F. Ding, J. Phys. Chem. Lett. **11**, 6235 (2020).

[24] Z. H. Zhang, Y. Yang, G. Y. Gao, and B. I. Yakobson, Angew. Chem., Int. Ed. **54**, 13022 (2015).

[25] A. J. Mannix, X. F. Zhou, B. Kiraly, J. D. Wood, D. Alducin, B. D. Myers, X. Liu, B. L. Fisher, U. Santiago, J. R. Guest,

M. J. Yacaman, A. Ponce, A. R. Oganov, M. C. Hersam, and N. P. Guisinger, Science **350**, 1513 (2015).

[26] B. J. Feng, J. Zhang, Q. Zhong, W. B. Li, S. Li, H. Li, P. Cheng, S. Meng, L. Chen, and K. H. Wu, Nat. Chem. **8**, 563 (2016).

[27] Q. Zhong, J. Zhang, P. Cheng, B. J. Feng, W. B. Li, S. X. Sheng, H. Li, S. Meng, L. Chen, and K. H. Wu, J. Phys.: Condens. Matter **29**, 095002 (2017).

[28] N. A. Vinogradov, A. Lyalin, T. Taketsugu, A. S. Vinogradov, and A. Prebrajenski, ACS Nano **13**, 14511 (2019).

[29] H. F. Wang, Q. F. Li, Y. Gao, F. Miao, X. F. Zhou, and X. G. Wan, New J. Phys. **18**, 073016 (2016).

[30] Y. X. Liu, Y. J. Dong, Z. Y. Tang, X. F. Wang, L. Wang, T. J. Hou, H. P. Lin, and Y. Y. Li, J. Mater. Chem. C **4**, 6380 (2016).

[31] L. Adamska, S. Sadasivam, J. J. Foley, P. Darancet, and S. Sharifzadeh, J. Phys. Chem. C **122**, 4037 (2018).

[32] Z. Zhang, Y. Yang, E. S. Penev, and B. I. Yakobson, Adv. Funct. Mater. **27**, 1605059 (2017).

[33] E. S. Penev, A. Kutana, and B. I. Yakobson, Nano Lett. **16**, 2522 (2016).

[34] Y. C. Zhao, S. M. Zeng, and J. Ni, Appl. Phys. Lett. **108**, 242601 (2016).

[35] M. Gao, Q. Z. Li, X. W. Yan, and J. Wang, Phys. Rev. B **95**, 024505 (2017).

[36] G. Li, Y. C. Zhao, S. M. Zeng, M. Zulfiqar, and J. Ni, J. Phys. Chem. C **122**, 16916 (2018).

[37] S. Er, G. A. de Wijs, and G. Brocks, J. Phys. Chem. C **113**, 18962 (2009).

[38] H. Jiang, Z. Lu, M. Wu, F. Ciucci, and T. Zhao, Nano Energy **23**, 97 (2016).

[39] X. M. Zhang, J. P. Hu, Y. C. Cheng, H. Y. Yang, Y. G. Yao, and S. Y. A. Yang, Nanoscale **8**, 15340 (2016).

[40] X. F. Zhou, A. R. Oganov, Z. H. Wang, I. A. Popov, A. I. Boldyrev, and H. T. Wang, Phys. Rev. B **93**, 085406 (2016).

[41] M. J. Aziz, E. Nygren, J. F. Hays, and D. Turnbull, J. Appl. Phys. **57**, 2233 (1985).

[42] T. Endo, T. Sato, and M. Shimada, J. Mater. Sci. Lett. **6**, 683 (1987).

[43] R. E. Youngman, S. T. Haubrich, J. W. Zwanziger, M. T. Janicke, and B. F. Chmelka, Science **269**, 1416 (1995).

[44] S. J. Hwang, C. Fernandez, J. P. Amoureux, J. Cho, S. W. Martin, and M. Pruski, Solid State Nucl. Magn. Reson. **8**, 109 (1997).

[45] D. He, Y. Zhao, L. Daemen, J. Qian, T. D. Shen, and T. W. Zerda, Appl. Phys. Lett. **81**, 643 (2002).

[46] H. T. Hall and L. A. Compton, Inorg. Chem. **4**, 1213 (1965).

[47] G. Ferlat, A. P. Seitsonen, M. Lazzeri, and F. Mauri, Nature Mater. **11**, 925 (2012).

[48] L. Z. Kou, Y. D. Ma, C. Tang, Z. Q. Sun, A. J. Du, and C. F. Chen, Nano Lett. **16**, 7910 (2016).

[49] R. Peköz, M. Konuk, M. E. Kilic, and E. Durgun, ACS Omega **3**, 1815 (2018).

[50] L. C. Xu, A. J. Du, and L. Z. Kou, Phys. Chem. Chem. Phys. **18**, 27284 (2016).

[51] Z. Q. Wang, T. Y. Lü, H. Q. Wang, Y. P. Feng, and J. C. Zheng, Phys. Chem. Chem. Phys. **18**, 31424 (2016).

[52] A. A. Kistanov, Y. Cai, K. Zhou, N. Srikanth, S. V. Dmitriev, and Y. W. Zhang, Nanoscale **10**, 1403 (2018).

[53] D. F. Li, J. He, G. Q. Ding, Q. Q. Tang, Y. Ying, J. J. He, C. Y. Zhong, Y. Liu, C. B. Feng, Q. L. Sun, H. Zhou, P. Zhou, and G. Zhang, Adv. Funct. Mater. **28**, 1801685 (2018).

[54] Z. Q. Wang, T. Y. Lu, H. Q. Wang, Y. P. Feng, and J. C. Zheng, ACS Appl. Electron. Mater. **1**, 667 (2019).

[55] Q. C. Li, V. S. C. Kolluru, M. S. Rahn, E. Schwenker, S. Li, R. G. Hennig, P. Darancet, M. K. Chan, and M. C. Hersam, Science **371**, 1143 (2021).

[56] G. Kresse and J. Furthmüller, Phys. Rev. B **54**, 11169 (1996).

[57] W. Kohn, A. D. Becke, and R. G. Parr, J. Phys. Chem. **100**, 12974 (1996).

[58] P. E. Blöchl, Phys. Rev. B **50**, 17953 (1994).

[59] J. P. Perdew and Y. Wang, Phys. Rev. B **46**, 12947 (1992).

[60] J. P. Perdew, K. Burke, and M. Ernzerhof, Phys. Rev. Lett. **77**, 3865 (1996).

[61] H. J. Monkhorst and J. D. Pack, Phys. Rev. B **13**, 5188 (1976).

[62] P. Giannozzi, S. Baroni, N. Bonini, M. Calandra, R. Car, C. Cavazzoni, D. Ceresoli, G. L. Chiarotti, M. Cococcioni, I. Dabo *et al.*, J. Phys.: Condens. Matter **21**, 395502 (2009).

[63] W. L. McMillan, Phys. Rev. **167**, 331 (1968).

[64] P. B. Allen, Phys. Rev. B **6**, 2577 (1972).

[65] P. B. Allen and R. C. Dynes, Phys. Rev. B **12**, 905 (1975).

[66] C. Cheng, J. T. Sun, H. Liu, H. X. Fu, J. Zhang, X. R. Chen, and S. Meng, 2DMater. **4**, 025032 (2017).

[67] See Supplemental Material at https://link.aps.org/supplemental/10.1103/PhysRevMaterials.7.034004 for the structural information of $\beta_{12}$ borophene and the hydrogenated $\beta_{12}$ borophenes in Fig. A1.

[68] C. Hou, G. Tai, J. Hao, L. Sheng, B. Liu, and Z. Wu, Angew. Chem. **132**, 10911 (2020).

[69] W. N. Lipscomb, Science **196**, 1047 (1977).

[70] J. A. Dagata, J. Schneir, H. H. Harary, C. J. Evans, M. T. Postek, and J. Bennett, Appl. Phys. Lett. **56**, 2001 (1990).

[71] J. W. Lyding, T. C. Shen, J. S. Hubacek, J. R. Tucker, and G. C. Abeln, Appl. Phys. Lett. **64**, 2010 (1994).

[72] C. R. Ryder, J. D. Wood, S. A. Wells, Y. Yang, D. Jariwala, T. J. Marks, G. C. Schatz, and M. C. Hersam, Nat. Chem. **8**, 597 (2016).

[73] H. Şahin, S. Cahangirov, M. Topsakal, E. Bekaroglu, E. Akturk, R. T. Senger, and S. Ciraci, Phys. Rev. B **80**, 155453 (2009).